Constructing Binary and Ternary Phase Diagrams on the Basis of Phase Stability Analysis

ARTICLE *in* INDUSTRIAL & ENGINEERING CHEMISTRY RESEARCH · JULY 2002

Impact Factor: 2.59 · DOI: 10.1021/ie0200499

Constructing Binary and Ternary Phase Diagrams on the Basis of Phase Stability Analysis

Sugata Pikatan Tan and Maciej Radosz*

Department of Chemical and Petroleum Engineering, University of Wyoming, Laramie, Wyoming 82071-3295

A phase stability approach to constructing phase diagrams is demonstrated for binary and ternary mixtures. This is an alternative to flash-calculation approaches, which tend to produce nonunique solutions. The new approach utilizes a recently proposed tangent-plane method coupled with an interval Newton algorithm.

Introduction

Understanding the phase behavior of mixtures is key to designing chemical reactors and separators. Phase diagrams are a common way to illustrate the phase behavior of mixtures. We refer to phase diagrams by the coordinates representing the thermodynamic parameters that are variable, for example, $P-T$, $P-xy$, or $T-xy$, etc., where P is the pressure, T is the temperature, and x and y are mole fractions. The phase diagrams show phase boundary curves that represent the conditions of phase transitions. The phase boundary curves are usually calculated using a flash-calculation approach that boils down to solving a set of simultaneous thermodynamic equations. For example, when an equation of state (EOS) is used for both phases, we have the following equations: (1) the equifugacity equations for each component, (2) an EOS relating the thermodynamics variables, and (3) the consistency equation of mass balance. When we refer to flash calculation in this paper, we mean a method that solves these equations alone.

A general issue associated with such a flash approach is that it cannot reliably produce a unique, physically meaningful solution; it typically produces multiple solution roots. Even simple cubic EOSs, such as van der Waals, Soave−Redlich−Kwong (SRK), and Peng−Robinson, may result in multiple solution roots.[1]

A practical issue associated with the flash approach is that it upfront requires a specific definition of the phases present, that is, the number and type of the phases present. In a way, this approach calls for an answer to get an answer. This is needed to interpret and select the calculated density values. For example, in the density calculation proposed by Topliss,[2] the density selection for the liquid−liquid equilibrium (LLE) is different from that for the vapor−liquid equilibrium (VLE). If we obtain three different density values and one of them can be eliminated on the basis of the mechanical instability, the flash routine still needs a clear instruction to determine which of the two remaining density values should be used for further calculations.

A conceptual issue associated with the flash approach is that the simultaneous equations underlying the flash routines, in fact, are the necessary but not sufficient conditions of the phase equilibria. The sufficient condition is that the Gibbs energy of the system must reach a minimum at a given pressure and temperature.[1] To satisfy this condition, one could, in principle, do a flash calculation followed by the Gibbs energy analysis to test the flash results. However, the conventional flash algorithms search the solution roots one at a time, which is initial-guess sensitive, and hence tend to miss some roots. Therefore, the flash approach, coupled with the Gibbs energy analysis using the conventional algorithms, does not guarantee a correct result, unless *all* of the existing flash solution roots are found and tested.

There have been many attempts documented in the literature to address the issues with the flash calculation described above. Typical recent examples include GLOPEQ,[3] the area method,[4] the homotopy-continuation algorithm,[5] the advanced flash algorithm by Lucia et al.,[6] etc. These examples utilize the Gibbs energy as the equilibrium criterion. The first two methods are robust and effective to deal with the equilibrium problems, except that their applicability is quite limited: for example, GLOPEQ can be used with the activity coefficient models only, and the area method is reliable for binaries only. Except for the area method, these methods utilize the minimization of the Gibbs energy. Lucia et al.[6] developed a reliable initialization algorithm. They creatively combine several initialization strategies toward determining a correct number of phases and the corresponding phase equilibrium compositions.

The goal of this work is to explore an alternative approach to constructing the phase diagrams: not on the basis of the flash calculations but on the basis of the phase stability analysis alone. This is possible by utilizing the recently proposed phase stability analysis using a tangent-plane (Gibbs energy)[1,7] method coupled with an interval algorithm.[8] The tangent-plane method was previously used for the phase stability analysis preceding the search of the global minimum of the Gibbs energy in the homotopy-continuation algorithm[5] and for identifying all of the immiscible binaries in the initialization step by Lucia et al.[6]

The interval method is promising for our purpose because it probes and diagnoses with certainty the stable (homogeneous) and unstable (heterogeneous) regions in the phase diagrams. The practical advantage of using the interval algorithm is twofold: no need for smart initial guesses and a certainty of finding the global minimum of the Gibbs energy. Although the tangent-plane method was originally envisioned as an

* Corresponding author. E-mail: Radosz@uwyo.edu. Tel: 307-766-2500. Fax: 307-766-6777.

10.1021/ie0200499 CCC: $22.00
Published on Web 06/28/2002

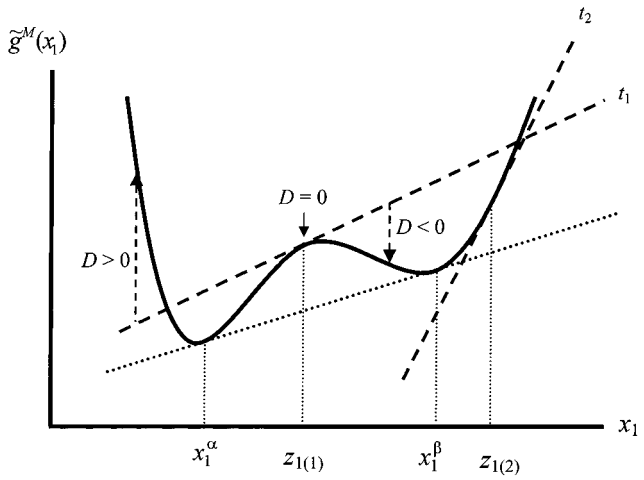

Figure 1. Reduced molar Gibbs energy of mixing versus mole fraction.

auxiliary phase stability test for the flash results, we shall use it as the only tool for predicting the phase boundaries and constructing the phase diagrams.

We shall test and illustrate this approach on a binary mixture that can form up to three phases, such as *n*-tetracontane (1)/propane (2). Normal tetracontane is a long-chain alkane ($C_{40}H_{82}$), which is treated here as a prototype of linear polyethylene. We also test this approach on a ternary mixture of ethane (1)/heptane (2)/butane (3). Because our target systems contain polymers, we use statistical associating fluid theory (SAFT)[9,10] as the working EOS. For the ternary, SRK EOS is also used for comparison purposes.

Tangent-Plane Method

A common probe of the mixture phase stability is the plane tangent to the Gibbs energy surface at the point of the overall mixture composition. If the tangent plane does not intersect the Gibbs surface, i.e., if none of its points can be found above the Gibbs surface, we declare the mixture to be stable. Such a stable mixture has no tendency to separate spontaneously into two or more phases. Conversely, if the tangent plane intersects the Gibbs surface, i.e., if some of its points can be found above the Gibbs surface, we declare the mixture to be unstable. Such an unstable mixture has a tendency to separate spontaneously into two or more phases.

For a special case of binary mixtures, the tangent plane reduces to a tangent line and the Gibbs surface reduces to a Gibbs curve, as shown in Figure 1, where the reduced molar Gibbs energy of mixing, $\tilde{g}^M$, shown as a solid curve, is plotted versus the mole fraction of component 1, x_1. The two dashed lines, t_1 and t_2, shown in Figure 1 are tangent to the Gibbs curve at the feed mole fractions $z_{1(1)}$ and $z_{1(2)}$, respectively; the feed $z_{1(1)}$ is unstable, and hence it will split into two phases, α and β, having the mole fractions of x_1^α and x_1^β, respectively, because its tangent line t_1 intersects the Gibbs surface. On the other hand, the feed $z_{1(2)}$ is stable, and hence it will remain as a one-phase fluid because its tangent line, t_2, does not intersect the Gibbs curve; it lies below it.

The phase stability problem can be framed as a minimization problem.[1,7] The objective function to be minimized is the distance from the tangent plane to the Gibbs surface:

$$D(\mathbf{x},\mathbf{z}) = \tilde{g}^M(\mathbf{x}) - \tilde{g}^M(\mathbf{z}) - \sum_{i=1}^{n}\left[\frac{\partial \tilde{g}^M}{\partial x_i}\right]_{\mathbf{x}=\mathbf{z}}(x_i - z_i) \quad (1)$$

where the bold symbols mean the mole fraction vectors, x_i and z_i mean mole fractions, and n means the number of components. For example, for a binary mixture, where $n = 2$, the mole fraction vector $\mathbf{x}$ consists of two components, x_1 and $x_2 = 1 - x_1$, and so does the feed mole fraction vector $\mathbf{z}$, which consists of z_1 and $z_2 = 1 - z_1$.

The goal of the minimization is to find the value of $\mathbf{x}$ that results in the global minimum of D. If the global minimum value of D is negative, the tangent plane must lie above the Gibbs surface at the vicinity of the minimum, and hence the mixture is declared to be unstable.

To minimize D, the first derivatives of $D(\mathbf{x})$ with respect to the mole fractions, that is, the gradient of D in the n-dimensional composition space, are set equal to zero

$$\left(\frac{\partial \tilde{g}^M}{\partial x_i} - \frac{\partial \tilde{g}^M}{\partial x_n}\right) - \left(\frac{\partial \tilde{g}^M}{\partial x_i} - \frac{\partial \tilde{g}^M}{\partial x_n}\right)_{\mathbf{x}=\mathbf{z}} = 0 \qquad i = 1, ..., n-1 \quad (2)$$

and solved subject to the consistency constraint:

$$1 - \sum_{i=1}^{n} x_i = 0 \quad (3)$$

For binaries, there is only one eq 2, while eq 3 becomes $1 - x_1 - x_2 = 0$. Along with an EOS, which relates the thermodynamic variables needed to calculate the Gibbs energy, eqs 2 and 3 form a set of three equations that need to be solved simultaneously. This method can be generalized to mixtures containing n components, for which $n + 1$ equations need to be solved simultaneously. The $n + 1$ independent variables are the n mole fractions and either the molar volume or the molar density of the mixture.

Such a system of simultaneous equations usually results in multiple solutions that correspond to the stationary points of D, such as minima, maxima, and inflection points, and in a trivial solution, $\mathbf{x} = \mathbf{z}$. The trivial solution represents a point tangent to the Gibbs surface where $D = 0$, and hence it is routinely rejected. The goal is to find a unique solution, which corresponds to the global minimum of D. The conventional algorithms, such as Newton−Raphson and steepest descent, which are initial-guess sensitive, often end up with a local minimum instead of the global minimum.

A more reliable alternative is a Newton method using interval mathematics.[8] Such an interval approach leads to finding *all* existing solution roots of the nonlinear simultaneous equations,[11,12] including the global minimum.

Interval Newton Method

Instead of using real numbers, x, the interval analysis approximates each variable in terms of an interval $\mathbf{x}$ characterized by the lower and upper bounds $[\underline{x}, \bar{x}]$. If the lower and upper bounds coincide, the interval reduces to the real number. The interval analysis, with

its own mathematics, is described in detail elsewhere, for example, in refs 12 and 13. The interval analysis used in this work is mostly based on the modules described in refs 14 and 15. In the overview below, a bold symbol means an interval (as opposed to the real number) and a capital symbol means a matrix (real or interval).

In general, one starts the calculation with a broad interval for each independent variable and one gradually narrows it down until the interval converges to a real number, which becomes the desired solution. When applied to calculating the physical properties, this interval method commonly starts with a physically reasonable range for each property, for example, 0−1 for mole fraction, which eliminates the need for "smart" initial guesses needed in the conventional numerical approaches.

The simultaneous equations to be solved using the Newton method can be lumped as an interval equation as follows:

$$\mathbf{J}(\mathbf{X}^k)(\tilde{\mathbf{X}}^k - X^k) = -\mathbf{F}(\mathbf{X}^k) \tag{4}$$

where $\mathbf{F}$ represents the interval extension of the simultaneous equations that need to be solved and $\mathbf{J}$ represents the Jacobian. The real vector X is the center of the interval vector $\mathbf{X} = (\mathbf{x}_1, \mathbf{x}_2, ..., \mathbf{x}_n)$, i.e., a set of the midpoints of intervals $\mathbf{x}_i$. Superscript k indicates the kth iteration in the computation. The main result of eq 4 is a new value of $\tilde{\mathbf{X}}^k$ which may or may not replace the old value of $\mathbf{X}^k$ as the next $\mathbf{X}^{k+1}$, subject to the following root inclusion tests:

1. If the new interval $\tilde{\mathbf{X}}^k$ turns out to be a subset of the old $\mathbf{X}^k$, there is exactly one solution in the interval. Therefore, a conventional root-searching routine can be applied to accelerate the process with $\mathbf{X}^{k+1} = \tilde{\mathbf{X}}^k$.

2. If $\tilde{\mathbf{X}}^k$ partially intersects (has a partial overlap with) $\mathbf{X}^k$, the existence of the solution remains undetermined. If solutions do exist in the interval, they will reside in the intersection, $\tilde{\mathbf{X}}^k \cap \mathbf{X}^k$. Therefore, $\mathbf{X}^{k+1} = \tilde{\mathbf{X}}^k \cap \mathbf{X}^k$ instead of using the whole range of $\tilde{\mathbf{X}}^k$.

3. If $\tilde{\mathbf{X}}^k$ does not intersect $\mathbf{X}^k$, no solution exists in the interval $\mathbf{X}^k$. Therefore, further search is abandoned for the interval.

Equation 4 is first preconditioned with a real matrix Y, called the preconditioner, which is often taken as the inverse of the Jacobian midpoints.[16] Then we convert the matrix equation (4) into algebraic equations using the Gauss−Seidel procedure:[11]

$$\mathbf{x}_i^k = x_i^k - \frac{1}{\mathbf{q}_{ii}^k}[\mathbf{h}_i^k + \sum_{\substack{j=1 \\ j\neq i}}^{n} \mathbf{q}_{ij}^k(\mathbf{x}_j^k - x_j^k)] \tag{5}$$

where $\mathbf{q}_{ij}$ values are the elements of the matrix product $Y\mathbf{J}$ and $\mathbf{h}_i$ values are the matrix product of Y_i, i.e., the ith row of Y, and $\mathbf{F}$: $Y_i\mathbf{F}$.

A decision whether to split an interval into two smaller parts, and further splits to find *all* of the existing solutions, is based on the interval value of denominator $\mathbf{q}_{ii}$ in eq 5. If the interval contains zero, i.e., when the lower bound is negative and the upper bound is positive, the old $\mathbf{X}^k$ must be split into two smaller intervals for further evaluation. The interval splitting process is a simple bisection if the terms in the parentheses in eq 5 contain zero. If not, the interval splitting process utilizes *Kahan*'s extended-interval procedure.[13] These interval splitting mechanisms, along with the root-inclusion tests described above, are the essential elements of the interval method used in this work. A detailed description of the algorithm can be found in Schnepper and Stadtherr.[16]

The interval tangent approach to the phase stability analysis has been applied to the excess Gibbs energy models (UNIQUAC and NRTL),[17] the cubic EOSs,[8] and a noncubic EOS called SAFT.[18]

SAFT EOS

The SAFT EOS is defined in terms of the dimensionless residual molar Helmholtz free energy (we shall drop the words residual, molar, and free from further references), which is usually expressed as the sum of hard-sphere, dispersion, chain, and association contributions:

$$\tilde{a}^{\text{res}} = \tilde{a}^{\text{hs}} + \tilde{a}^{\text{disp}} + \tilde{a}^{\text{chain}} + \tilde{a}^{\text{assoc}} \tag{6}$$

For nonassociating mixtures, such as *n*-tetracontane (1)/propane (2), the association term can be dropped from the right-hand side of eq 6. A detailed description of SAFT can be found in Huang and Radosz.[9,10]

The reduced molar Gibbs energy change of mixing in eqs 1 and 2 can be calculated from the residual Helmholtz energy:

$$\tilde{g}^{\text{M}}(\mathbf{x}) = \tilde{a}^{res}(\mathbf{x}) + Z(\mathbf{x}) - \ln v(\mathbf{x}) - \sum_{i=1}^{n} x_i(\tilde{a}_i^{\text{res}} + Z_i - \ln x_i v_i) \tag{7}$$

where $v(\mathbf{x})$ is the molar volume of the mixture, $Z(\mathbf{x})$ is the compressibility factor for the mixture, Z_i is the compressibility factor for pure component i, v_i is the molar volume, and $\tilde{a}_i^{\text{res}}$ is the residual Helmholtz energy of pure component i. The relation between composition and volume, as needed in eq 7, is given by

$$\rho(\mathbf{x})\left(\frac{\partial \tilde{a}^{res}}{\partial \rho}\right)_{T,x} = Z(\mathbf{x}) - 1 \tag{8}$$

where $\rho(\mathbf{x})$ is the molar density of the mixture, the inverse of the molar volume.

Xu et al.[18] selected the molar component densities, $\rho_i = \rho x_i$ as the independent variables. Instead, we select the reduced fluid density, η, as the independent variable accompanying the mole fractions x_i. The reduced fluid density is the SAFT segment packing fraction

$$\eta = \frac{\pi}{6} N_{\text{A}} \rho \sum_{i=1}^{n} x_i m_i {d_i}^3 \tag{9}$$

where m_i is the segment number of component i, d_i is the temperature-dependent segment diameter of component i in the mixture, and N_{A} is Avogadro's number. The advantage of using the segment packing fraction is that we know its physical upper limit given by the close packing of spheres, i.e., $\tau = 0.740\,48$.

However, with an interval initial value of $\eta = [0, \tau]$, the SAFT dispersion term tends to be excessively overestimated, which causes computational difficulties. The dispersion term is a power series[19] in η

$$\tilde{a}^{\text{disp}} = (\sum_{i=1}^{n} x_i m_i) \sum_{j=1}^{4} \sum_{k=1}^{9} D_{jk} \left(\frac{u}{\kappa T}\right)^j \left(\frac{\eta}{\tau}\right)^k \tag{10}$$

where D_{jk} are the universal constants, u is the energy-dependent internal energy, and κ is the Boltzmann constant.

Fortunately, the interval width of the dispersion term, eq 10, can be greatly reduced for fluids on the basis of a fluid-to-solid transition for hard spheres[20] around $\eta = 0.45$. It is, therefore, safe to estimate the upper limit to be 0.4 for real fluids. The lower limit is assigned a small but nonzero value to avoid singularities. In this work, the initial interval of η is set as $[10^{-4}, 0.4]$ and the initial interval of x_i is set as $[10^{-13}, 1]$. Alternatively, one could choose lower limits corresponding to the ideal gas volume for η, but there is no practical computational advantage found for such a physical refinement.

The shorter intervals introduced above allow for a streamlined version of eq 10

$$\tilde{a}^{\text{disp}} = \left(\sum_{i=1}^{n} x_i m_i\right)\sum_{j=1}^{4} c_j \left(\frac{u}{\kappa T}\right)^j \tag{11}$$

where the η-dependent coefficients c_j are evaluated as follows:

$$c_j = \sum_{k=1}^{9} D_{jk}\left(\frac{\eta}{\tau}\right)^k \tag{12}$$

Because these coefficients are polynomials in η, their actual bounds, and those of their derivatives with respect to η, are easily determined when a particular interval of η is in use.

Developing a Phase Diagram Using Phase Stability Analysis

The first step in developing a phase diagram is to select its coordinates. For example, when we set the temperature to be constant, we usually plot $P-xy$ phase boundaries. This can be accomplished by scanning the whole $P-xy$ region of interest for phase stability, that is, by tracking the sign of the minimum value of D, D_{min}, at each point of the grid; as usual, we routinely disregard the trivial solution root. A change of sign of D_{min} in going from one point to another indicates that we cross a phase boundary. If we start in a one-phase (stable) region, for example, then a change of the sign of D_{min} from positive to negative signifies a phase boundary between the one- and two-phase regions, a one-to-two phase transition.

To find an exact value of the phase boundary between the grid points, one can apply a linear interpolation routine. This is straightforward because the D values of solution roots, i.e., all of the stationary values of D, tend to be continuous functions of the independent variables in the vicinity of the phase boundaries. For example, for the $P-xy$ diagram, they can be plotted as piecewise continuous curves in the D versus z_1 coordinates, as will be illustrated in the next section. In the interpolation step, one determines the z_1 point at which D_{min} becomes zero. Such a z_1 point represents a phase boundary for a given P. Once the phase boundary points are found for a given P, the procedure is repeated for a new P. Finally, all of the phase boundary points are collected and replotted in the form of a $P-xy$ phase diagram. This procedure can easily be automated so that each new $P-xy$ phase diagram can be developed essentially in one step. A similar procedure can be used to develop $T-xy$ and $P-T$ phase diagrams.

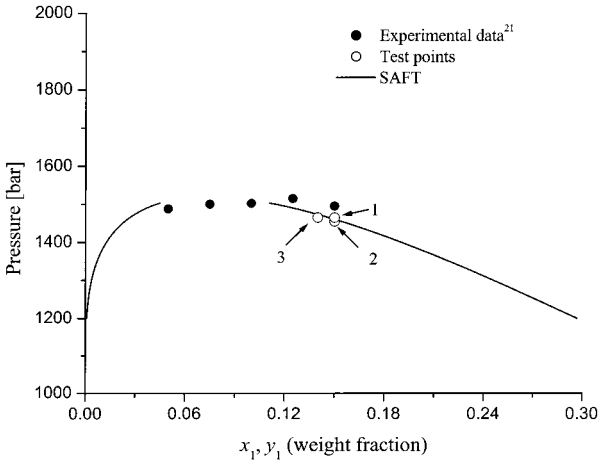

Figure 2. $P-xy$ diagram of polymer NIST 1483 (1)/ethylene (2) at $T = 433.15$ K.

Results and Discussion

Before we present examples illustrating the phase stability approach described in the previous section, we present an example of a phase diagram obtained from a conventional flash method to illustrate the point that, however unreliable in general, the flash method can produce useful results as long as they are tested for phase stability. This example is for a binary mixture of linear polyethylene (1) and ethylene (2), where polyethylene is NIST 1483. Because this is a binary system, we can use TP flash calculations; the TP flash results coincide with the bubble- or dew-flash results and hence can be used to determine the phase boundaries. Figure 2 shows a $P-xy$ diagram for this mixture at 433.15 K, where the curves represent the flash calculation and the solid points represent the experiment reported by Chan et al.[21] (where the NIST 1483 sample is labeled EO-0-30). The SAFT parameters and the binary interaction parameter are also taken from Chan et al.[21] The phase diagram calculated from the SAFT flash program is tested for phase stability. A sample of such a phase stability test is shown with three open-circle points in the vicinity of the phase boundary curve. If the flash results are physically meaningful, we expect point 1 to be in the one-phase region (to represent a stable phase) and points 2 and 3 to be in the two-phase region (to represent an unstable phase).

The phase stability results can be characterized in terms of the tangent-plane distance, D, plotted versus weight fraction in Figure 3. The D curves in Figure 3 are truncated beyond $x_1 = 0.18$, where they are positive and increase monotonically. Figure 3 suggests that the test-point 1 (corresponding to point 1 in Figure 2) is the only point that lies in the one-phase region at 433.15 K because the corresponding D curve in Figure 3 is never negative for all x_1. On the other hand, the D values of test-points 2 and 3 have negative global minima indicated by the arrows in Figure 3. This means that both points 2 and 3 are in the two-phase region at 433.15 K. These results confirm that the 433.15 K phase boundary calculated from the flash method should be correct.

An alternative approach to the phase stability analysis is to calculate all of the extrema of D using the interval algorithm. The results are presented in Table

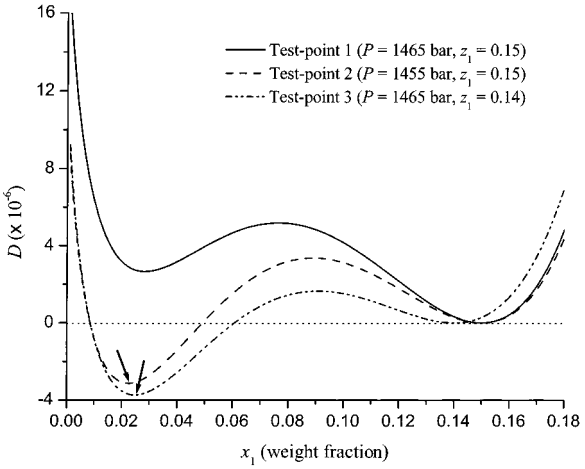

Figure 3. Tangent-plane distance D vs polymer weight fraction x_1 for the three test points in Figure 2.

Table 1. Phase Stability Analysis of Polymer NIST 1483 (1)/Ethylene (2) at T = 433.15 K (x_1 and z_1 Are Weight Fractions)

test point	roots: (x_1, η)	D	status	CPU time[a] (s)
1 (P = 1465 bar; z_1 = 0.15)	(0.0283, 0.3166)	2.65×10^{-6}	stable	1374
	(0.0764, 0.3184)	5.18×10^{-6}		
	(0.1500, 0.3212)	0		
2 (P = 1455 bar; z_1 = 0.15)	(0.0225, 0.3159)	-3.13×10^{-6}	unstable	1387
	(0.0889, 0.3183)	3.36×10^{-6}		
	(0.1500, 0.3207)	0		
3 (P = 1465 bar; z_1 = 0.14)	(0.0248, 0.3165)	-3.73×10^{-6}	unstable	1461
	(0.0908, 0.3189)	1.64×10^{-6}		
	(0.1400, 0.3208)	0		

[a] Intel Pentium 4 (1.8 MHz).

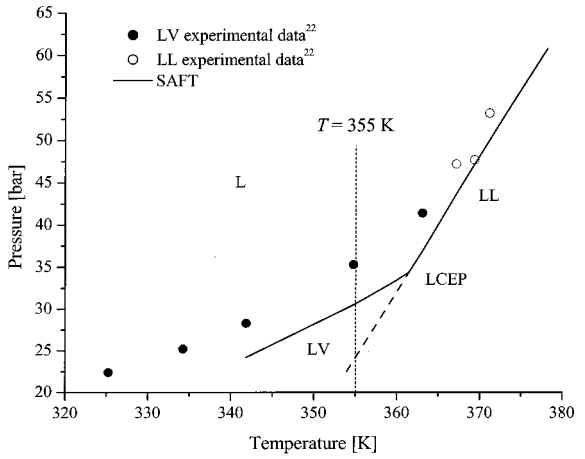

Figure 4. $P-T$ diagram for n-tetracontane (1)/propane (2) at z_1 = 7.13% by weight.

1, including the accurate values of the global minima qualitatively pointed out by the arrows in Figure 3. The entries are obtained by solving simultaneously eqs 2, 3, and 8. Each solution root represents a stationary point of the objective function, namely, D. The trivial solution, which gives D = 0, is the local minimum for test-points 2 and 3.

Our second example concerns VLE and LLE for a mixture of n-tetracontane (1) and propane (2), 7.13% by weight of n-tetracontane,[22] shown in Figure 4. The SAFT parameters for n-tetracontane are taken from Chan et al.,[23] whereas those for propane are taken from Huang and Radosz.[9] The binary interaction parameter,

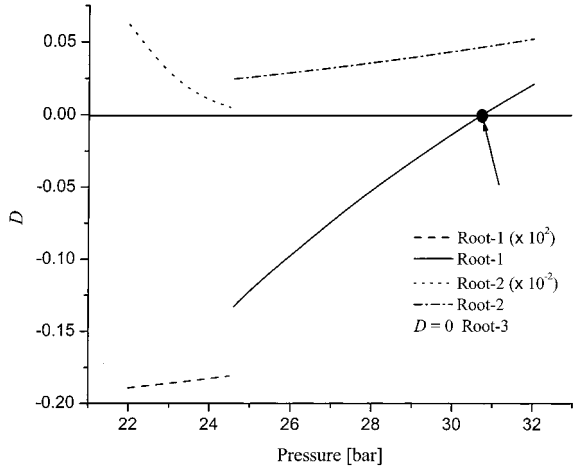

Figure 5. $D-P$ diagram of n-tetracontane (1)/propane (2) at T = 355 K and a feed of z_1 = 7.13% by weight.

k_{ij}, is set equal to zero because the accuracy of representing the experimental data is not crucial in this case.

The phase boundaries consist of two parts, i.e., LV at lower temperatures and LL at upper temperatures, with an intercept labeled LCEP (lower critical end point). These boundaries are commonly calculated from a series of flash calculations at constant temperature, in which the pressure is systematically varied until the light-phase fraction ("fraction vaporized" for VLE) becomes 1 (dew point) or 0 (bubble point). This is analogous to a dew-pressure or bubble-pressure VLE flash. To illustrate the problem associated with using such conventional flash routines, let us assume that we start the flash calculations at higher temperatures, on the LL side. As we proceed toward lower temperatures, the flash routine is likely to extrapolate the LL curve to physically unrealistic temperatures, beyond LCEP, as is shown with a dashed line in Figure 4. For example, an LLE flash calculation at T = 355 K easily converges to a dew-point-like transition at P = 22.95 bar. In fact, the transition is experimentally found to be of the bubble-point type and predicted at P = 30.72 bar from a VLE flash.

This sort of ambiguity can be eliminated using the interval Newton phase stability analysis. Solving eqs 2, 3, and 8, we observe three solution roots, including the trivial root that gives us D = 0. We can plot a $D-P$ diagram at T = 355 K, as shown in Figure 5. Because we need to pay attention to the minimum D value of a nontrivial root only, we focus on root-1 in Figure 5. Root-1 changes its sign at P = 30.72 bar (pointed out by the arrow in Figure 5), which is the phase boundary point in a $P-T$ diagram, and happens to be consistent with the VLE flash result. The discontinuity at P = 24.51 bar has no effect on the interpolation procedure near the phase boundary. This example is to illustrate that, in contrast to the conventional flash calculations, the phase stability analysis leads to an unambiguous diagnosis of the phase transitions.

Our third example amplifies this point for a $P-xy$ diagram of the same system at T = 365 K. As a point of reference, the results of the conventional TP flash calculations (three VLE cases and one LLE case) at P = 36.475 bar are presented in Table 2 in terms of weight fractions. Table 2 presents the equilibrium-phase weight fractions, $\mathbf{x}^{\alpha}$ and $\mathbf{x}^{\beta}$, and the overall molar fraction of phase β (called "fraction vaporized" for VLE).

Table 2. Weight Fraction Vectors Obtained from Conventional Flash Calculations (Three VLE Cases and One LLE Case) for *n*-Tetracontane (1)/Propane (2) at $P = 36.475$ bar and $T = 365$ K, Where Phase β Corresponds to a Vapor or Upper Liquid Phase

			mole fraction of phase β	
initial guess[a] $\mathbf{x}^{\alpha}$ (wt frac)	phase α $\mathbf{x}^{\alpha}$ (wt frac)	phase β $\mathbf{x}^{\beta}$ (wt frac)	$\mathbf{z}$ (wt frac) = (0.02, 0.98)	$\mathbf{z}$ (wt frac) = (0.06, 0.94)
(0.07, 0.93)	(0.0251, 0.9749)	($<10^{-4}$, 1)	0.2071	−1.4720[b]
(0.10, 0.90)	(0.1599, 0.8401).	($<10^{-4}$, 1)	0.8914	0.6614
(0.30, 0.70)	(0.2618, 0.7382)	($<10^{-4}$, 1)	0.9409	0.8159
(0.30, 0.70)[c]	(0.2819, 0.7181)	(0.0439, 0.9561)	1.0758[b]	0.9471

[a] The initial guess for $\mathbf{x}^{\beta}$ (weight) is (0.01, 0.99) for all cases. [b] Molar fractions of phase β are found to be outside of the allowable range (0−1), which indicates that the corresponding $\mathbf{x}^{\alpha}$ and $\mathbf{x}^{\beta}$ roots are unphysical. [c] This is an LLE flash case.

Table 3. Phase Stability Analysis of *n*-Tetracontane (1)/Propane (2) at $P = 36.475$ bar and $T = 365$ K

$\mathbf{z}$ (wt frac)	roots: (x_1, η)	D	status	CPU time[a] (s)
(0.02, 0.98)	(4.15×10^{-11}, 0.0496)	-1.81×10^{-4}	unstable	17.9
	(1.69×10^{-7}, 0.1055)	0.0214		
	(1.60×10^{-3}, 0.1971)	0		
(0.06, 0.94)	(6.02×10^{-11}, 0.0496)	7.77×10^{-4}	unstable	54.0
	(2.45×10^{-7}, 0.1055)	0.0224		
	(4.97×10^{-3}, 0.2087)	0		
	(8.46×10^{-3}, 0.2178)	2.69×10^{-5}		
	(3.54×10^{-2}, 0.2558)	-1.51×10^{-3}		

[a] Intel Pentium 4 (1.8 MHz).

As usually happens with the conventional flash calculations, different initial guesses lead to different solutions. For example, for the feed of $z_1 = 0.02$ (2% by weight *n*-tetracontane), the VLE routine results in three solutions corresponding to the three different initial guesses for $\mathbf{x}^{\alpha}$. All of these three solutions result in the overall phase β fractions that seem to be physically reasonable, in the 0−1 range. On the other hand, for the feed of $z_1 = 0.06$ (6% by weight *n*-tetracontane), one of the three roots has an unphysical overall phase β fraction, and hence it can be eliminated. A similar analysis of the overall phase β fraction for the LLE case (bottom of Table 2) suggests that the solution for the feed of $z_1 = 0.02$ is unphysical. In general, the analysis of the overall phase β mole fraction may eliminate some unphysical flash solutions, and only for some feed compositions, but it cannot eliminate all unphysical solutions that the flash calculations may produce.

By contrast, the phase stability analysis leads to unambiguous phase boundaries directly. Table 3 presents an example of such an analysis for the same binary of *n*-tetracontane (1)/propane (2). Any negative stationary D values immediately tell us that the system is unstable. An absence of negative stationary D values tells us that the system is stable.

The results presented in Table 3 happen to be qualitatively consistent with those presented in Table 2: both mixtures are found to be unstable. However, to determine systematically all of the phase boundaries, we need to scan the stationary D values for the whole range of the feed mole fraction, i.e., from 0 to 1. These values are plotted in $D-z$ coordinates in Figure 6; the lowest value of D at any given z_1 represents the global minimum of D for that z_1. Starting from $z_1 = 0.0385$, we find five roots, instead of three, including the trivial root.

As we can see in Figure 6, the D value of root-2 is always positive; thus, it has no effect on the mixture phase stability. On the other hand, root-1 is a nontrivial root giving the minimum D value, up to $z_1 = 0.0244$ where the D value is changing sign from negative to

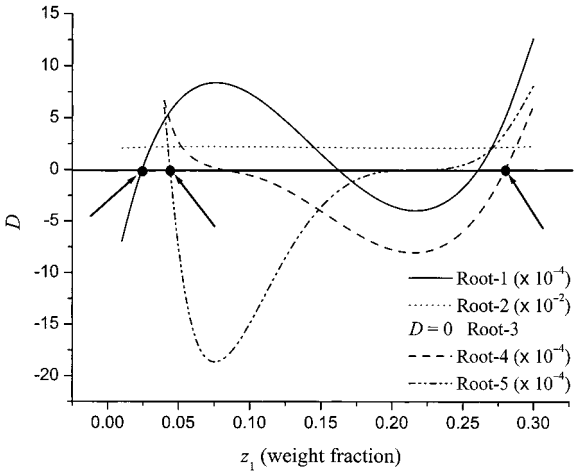

Figure 6. $D-z$ diagram of tetracontane (1)/propane (2) at $P = 36.475$ bar and $T = 365$ K.

positive. Then, root-5 and root-4 take turns giving the global minimum of D from $z_1 = 0.0439$ until $z_1 = 0.2819$; therefore, the mixture is unstable in this range (the global minimum is negative). The three weight fractions above, pointed out by arrows in Figure 6, are the physical phase boundaries of the mixture at $P = 36.475$ bar and $T = 365$ K. They quantitatively match the entries in Table 2 obtained from conventional flash calculation, except for 0.0244, where the small discrepancy is the result of a numerical inaccuracy of the conventional flash calculation most likely caused by the nonzero fraction of tetracontane in the vapor phase. The main difference between the two approaches is that the phase stability approach requires no assumptions regarding the number of phases beforehand and it leads to unambiguous answers.

If one repeats the same process at other pressures, scanning the whole pressure range of interest, one obtains a set of mole fractions that represent the phase boundaries. A plot in Figure 7 presents a set of such phase boundaries in the form of a complete $P-xy$ phase diagram for *n*-tetracontane (1)/propane (2) at $T = 365$ K in the 34−40 bar pressure range.

The regions bordered by the phase boundaries in Figure 7 are analogous to those in a common VLLE phase diagram and hence can be identified as follows: three unstable regions (VL^{α}, $L^{\alpha}L^{\beta}$, and VL^{β}) and two stable regions (L^{α} and L^{β}). One stable region, the vapor region, is not shown because it nearly coincides with the P axis ($y_1 = 0$); the vapor phase is essentially pure propane. The solid curve on the right-hand side of Figure 7 exhibits a change in slope at $P = 36.43$ bar where a horizontal line represents the LLV boundary.

This approach can be readily extended to multicomponent mixtures. This is illustrated for a ternary

Table 4. Phase Stability Analysis of Ethane (1)/Heptane (2)/Butane (3) at P = 48.26 bar and T = 394.26 K Using SRK and SAFT EOSs

	SAFT			SRK		
z_1/z_2 (mol frac)	x_1/x_2 (mol frac)	D	CPU time[a] (s)	x_1/x_2 (mol frac)	D	CPU time[a] (s)
0.90/0.04	0.5507/0.3435	0.1094	193.3			1.4
	0.7027/0.1921	0.1391				
	0.9/0.04	0		0.9/0.04	0	
0.6/0.2	0.8624/0.0269	−0.1552	563.4	0.8180/0.0481	−0.0809	2.7
	0.6366/0.1693	0.0005		0.5107/0.2787	−0.0041	
	0.6/0.2	0		0.6/0.2	0	

[a] Intel Pentium 4 (1.8 MHz).

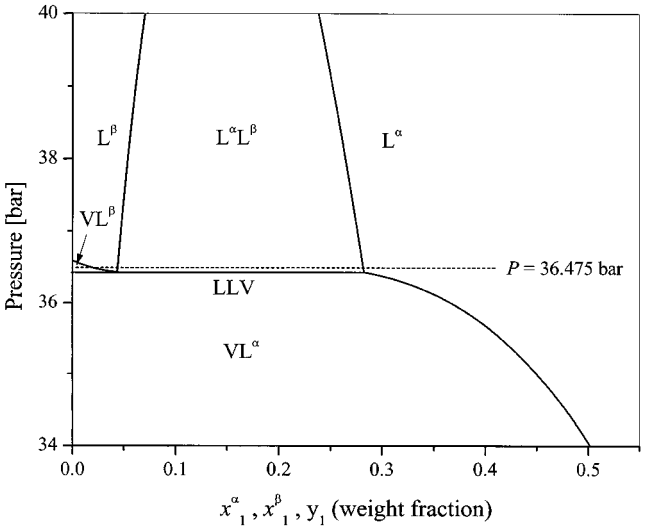

Figure 7. $P-xy$ diagram of n-tetracontane (1)/propane (2) at T = 365 K.

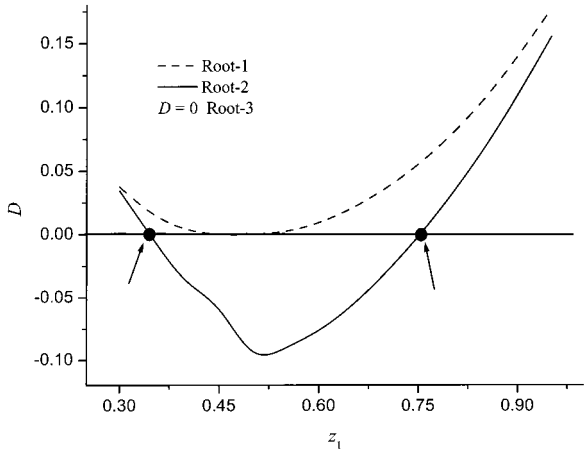

Figure 8. $D-z$ diagram of ternary ethane (1)/heptane (2)/butane (3) at P = 48.26 bar, T = 394.26 K, and z_2 = 0.04 using SAFT EOS.

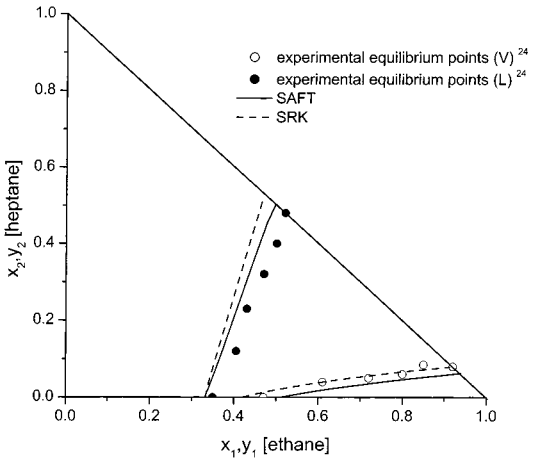

Figure 9. Phase diagram of ternary ethane (1)/heptane (2)/butane (3) at P = 48.26 bar and T = 394.26 K.

mixture of ethane (1)/heptane (2)/butane (3), for which there are experimental phase equilibrium data available.[24] For this ternary, we compare two equations of state, SRK and SAFT. The SRK parameters are taken from ref 25. The SAFT parameters for the three components are taken from Huang and Radosz.[9] The binary interaction parameters, k_{ij}, are set equal to zero for both equations of state. Table 4 shows the phase stability analysis using both equations of state at two points: z_1/z_2 = 0.9/0.04 and 0.06/0.20, at P = 48.26 bar and T = 394.26 K. A systematic phase stability scan using SAFT at constant P (=48.26 bar) and T (=394.26 K), and the overall mole fraction of heptane z_2 (=0.04), leads to a $D-z$ diagram shown in Figure 8. This procedure produces two nontrivial solution roots (roots 1 and 2) and a trivial root (root 3). Tracking the minimum D value of the nontrivial roots (solid curve root-2 in Figure 8), we find two phase boundaries, i.e., at x_1 = 0.3458 and x_1 = 0.7524 (pointed out with arrows in Figure 8), which bracket the unstable region. We repeat this process for other values of z_2 and plot the phase boundary points in a triangular phase diagram shown in Figure 9.

Examples of the phase stability analysis have been demonstrated for up to five-component mixtures.[17] However, phase diagrams for more than three components call for more than three dimensions and hence are awkward to present. In practice, therefore, we usually lump certain components and present binary or ternary phase diagrams in terms of two or three pseudocomponents.

Finally, we have a comment regarding efficiency: the approaches proposed in this work are reliable but are computation intensive. For example, with a step size of Δx_1 = 0.01, except in the vicinity of phase boundaries where the interpolation works, SAFT takes approximately 1 h of the CPU time to generate Figure 6 (up to x_1 = 1), while SRK needs approximately 2 h to complete Figure 9. As is shown in Tables 1, 3, and 4, the CPU time is strongly system dependent. For example, the system containing polymer requires much more time primarily because the polymer mole fraction has very low values; we find that the time needed for convergence increases with increasing asymmetry in magnitude of the mole fractions. Another factor is the complexity and nonlinearity of the EOS: SAFT calculations are much longer than the SRK calculations.

Conclusion

The phase stability analysis utilizing a tangent-plane method coupled with the interval Newton algorithm is found to be a reliable and complete approach to constructing the binary and ternary phase diagrams. In one step, one can simultaneously determine not only the phase stability of each region but also the corresponding phase boundaries. This approach eliminates the ambiguity associated with the conventional flash calculations, such as uncertain diagnosis of multiphase equilibria, multiple roots, and lacking roots and the need for smart initial guesses. However, this approach is CPU-time intensive, especially for multicomponent and asymmetric mixtures, such as polymer-containing mixtures.

Acknowledgment

We are grateful to Dr. Hertanto Adidharma for his useful suggestions and the computer codes of conventional flash calculation for SAFT used here. This work is funded by NSF Grant 9908610.

Notation

Roman Letters

$\tilde{a}^{res}$ = dimensionless residual molar Helmholtz free energy
c_j = η-dependent coefficients in SAFT dispersion term
d_i = temperature-dependent segment diameter of component i
D = distance from the tangent plane to the Gibbs energy surface
D_{jk} = universal constants in the SAFT dispersion term
$\mathbf{F}$ = interval extension vector of simultaneous equations
$\tilde{g}^{M}$ = reduced molar Gibbs energy change of mixing
$\tilde{g}_i^{0}$ = reduced molar Gibbs energy of pure component i
$\mathbf{h}_i$ = matrix product $Y_i\mathbf{F}$
$\mathbf{J}$ = interval Jacobian matrix
m_i = segment number of component i
n = number of components in the mixture
N_A = Avogadro's number
P = pressure
$\mathbf{q}_{ij}$ = elements of matrix product $Y\mathbf{J}$
t_i = tangent lines in the Gibbs energy diagram
T = absolute temperature
u = temperature-dependent internal energy
v = molar volume of the mixture
v_i = molar volume of pure component i
x_i = molar fraction of component i (weight fraction if it is mentioned so)
$\mathbf{x}$ = molar fraction vector (weight fraction if it is mentioned so)
$\mathbf{x_i}$ = interval entity serving as an element of interval vector $\mathbf{X}$
X = real vector, the elements of which are midpoints of $\mathbf{X}$
$\mathbf{X}$ = interval vector
y = molar fraction in the vapor phase (weight fraction if it is mentioned so)
Y = preconditioner matrix
z_i = feed molar fraction of component i (weight fraction if it is mentioned so)
$\mathbf{z}$ = feed molar fraction vector (weight fraction if it is mentioned so)
Z_i = compressibility factor of pure component i
Z = compressibility factor of the mixture

Greek Letters

η = reduced fluid density (segment packing fraction)
κ = Boltzmann constant
ρ = molar density of the mixture
τ = close-packing fraction of spheres

Literature Cited

(1) Baker, L. E.; Pierce, A. C.; Luks, K. D. Gibbs Energy Analysis of Phase Equilibria. *Soc. Pet. Eng. J.* **1982**, *22*, 731.

(2) Topliss, R. J. Techniques to Facilitate the Use of Equations of State for Complex Fluid-Phase Equilibria. Ph.D. Dissertation, University of California, Berkeley, CA, 1985.

(3) McDonald, C. M.; Floudas, C. A. GLOPEQ: A new computational tool for the phase and chemical equilibrium problem. *Comput. Chem. Eng.* **1997**, *21*, 1.

(4) Elhassan, A. E.; Tsvetkov, S. G.; Craven, R. J. B.; Stateva, R. P.; Wakeham, W. A. A Rigorous Mathematical Proof of the Area Method for Phase Stability. *Ind. Eng. Chem. Res.* **1998**, *37*, 1483.

(5) Sun, A. C.; Seider, W. D. Homotopy-continuation for the stability analysis in global minimization of the Gibbs free energy. *Fluid Phase Equilib.* **1995**, *103*, 213.

(6) Lucia, A.; Padmanabhan, L.; Venkataraman, S. Multiphase equilibrium flash calculations. *Comput. Chem. Eng.* **2000**, *24*, 2557.

(7) Michelsen, M. L. The isothermal flash problem. Part I. Stability. *Fluid Phase Equilib.* **1982**, *9*, 1.

(8) Hua, J. Z.; Brennecke, J. F.; Stadtherr, M. A. Enhanced Interval Analysis for Phase Stability: Cubic Equation of State Models. *Ind. Eng. Chem. Res.* **1998**, *37*, 1519.

(9) Huang, S. H.; Radosz, M. Equation of State for Small, Large, Polydisperse, and Associating Molecules. *Ind. Eng. Chem. Res.* **1990**, *29*, 2284.

(10) Huang, S. H.; Radosz, M. Equation of State for Small, Large, Polydisperse, and Associating Molecules: Extension to Fluid Mixtures. *Ind. Eng. Chem. Res.* **1991**, *30*, 1994.

(11) Kearfott, R. B. Interval Arithmetic Techniques in the Computational Solution of Nonlinear Systems of Equations: Introduction, Examples, and Comparisons. *Lect. Appl. Math.* **1990**, *26*, 337.

(12) Kearfott, R. B. *Rigorous Global Search: Continuous Problems*; Kluwer Academic Publishers: Dordrecht, The Netherlands, 1996.

(13) Hansen, E. R. *Global Optimization Using Interval Analysis*; Marcel Dekker: New York, 1992.

(14) Kearfott, R. B.; Dawande, M.; Du, K.-S.; Hu, C.-Y. Algorithm 737: INTLIB, a portable FORTRAN 77 Interval Standard Function Library. *ACM Trans. Math. Software* **1994**, *20*, 447.

(15) Kearfott, R. B. Algorithm 763; INTERVAL_ ARITHMETIC: a Fortran 90 Module for an Interval Data Type. *ACM Trans. Math. Software* **1996**, *22*, 385.

(16) Schnepper, C. A.; Stadtherr, M. A. Robust Process Simulation using Interval Methods. *Comput. Chem. Eng.* **1996**, *20*, 187.

(17) Tessier, S. R.; Brennecke, J. F.; Stadtherr, M. A. Reliable Phase Stability Analysis for Excess Gibbs Energy Models. *Chem. Eng. Sci.* **2000**, *55*, 1785.

(18) Xu, G.; Brennecke, J. F.; Stadtherr, M. A. Reliable Computation of Phase Stability and Equilibrium from the SAFT Equation of State. *Ind. Eng. Chem. Res.* **2002**, *41*, 938.

(19) Chen, S. S.; Kreglewski, A. Applications of the Augmented van der Waals Theory of Fluids. I. Pure Fluids. *Ber. Bunsen-Ges. Phys. Chem.* **1977**, *81*, 1048.

(20) Koak, N.; de Loos, T. W.; Heidemann, R. A. Effect of the Power Series Dispersion Term on the Pressure−Volume Behavior of Statistical Associating Fluid Theory. *Ind. Eng. Chem. Res.* **1999**, *38*, 1718.

(21) Chan, A.; Adidharma, H.; Radosz, M. Fluid−Liquid Transitions of Poly(ethylene-*co*-octene-1) in Supercritical Ethylene Solutions. *Ind. Eng. Chem. Res.* **2000**, *39*, 4370.

(22) Luszczyk, M.; Radosz, M. Temperature- and Pressure-Induced Crystallization and Melting of Tetracontane in Propane. Submitted for publication in *J. Chem. Eng. Data*.

(23) Chan, A.; Hemmingsen, P. V.; Radosz, M. Fluid−Liquid and Fluid−Solid Transitions of Tetracontane in Propane. *J. Chem. Eng. Data* **2000**, *45*, 362.

(24) Blas, F. J.; Vega, L. F. Prediction of Binary and Ternary Diagrams Using the Statistical Associating Fluid Theory (SAFT) Equation of State. *Ind. Eng. Chem. Res.* **1998**, *37*, 660.

(25) Smith, J. M.; Van Ness, H. C.; Abbott, M. M. *Introduction to Chemical Engineering Thermodynamic*, 6th ed.; McGraw-Hill Co., Inc.: New York, 2001.

Received for review January 15, 2002
Revised manuscript received May 17, 2002
Accepted May 21, 2002

IE0200499